Monthly Notices
of the
ROYAL ASTRONOMICAL SOCIETY

MNRAS **495,** 637–649 (2020)
Advance Access publication 2020 March 13

doi:10.1093/mnras/staa680

A spectroscopic analysis of the eclipsing nova-like EC 21178−5417 – discovery of spiral density structures

Z. N. Khangale [1,2★] P. A. Woudt,[1] S. B. Potter [2] B. Warner,[1] D. Kilkenny[3] and K. van der Heyden[1]

[1]*Department of Astronomy, University of Cape Town, Private Bag X3, Rondebosch 7701, South Africa*
[2]*South African Astronomical Observatory, PO Box 9, Observatory 7935, Cape Town, South Africa*
[3]*Department of Physics and Astronomy, University of the Western Cape, Private Bag X17, Bellville 7535, South Africa*

Accepted 2020 March 6. Received 2020 March 6; in original form 2019 March 11

ABSTRACT

We present phase-resolved optical spectroscopy of the eclipsing nova-like cataclysmic variable EC 21178−5417 obtained between 2002 and 2013. The average spectrum of EC 21178−5417 shows broad double-peaked emission lines from He II 4686 Å (strongest feature) and the Balmer series. The high-excitation feature, C III/N III at 4640–4650 Å, is also present and appears broad in emission. A number of other lines, mostly He I, are clearly present in absorption and/or emission. The average spectrum of EC 21178−5417 taken at different months and years shows variability in spectral features, especially in the Balmer lines beyond Hγ, from pure line emission, mixed line absorption, and emission to pure absorption lines. Doppler maps of the He II 4686 Å emission reveal the presence of a highly inclined asymmetric accretion disc and a two spiral arm-like structure, whereas that of the Balmer lines (Hα and Hβ) reveal a more circular accretion disc. There is no evidence of a bright-spot in the Doppler maps of EC 21178−5417 and no emission from the secondary star is seen in the tomograms of the He II 4686 Å and Balmer lines. Generally, the emission in EC 21178−5417 is dominated by emission from the accretion disc. We conclude that EC 21178−5417 is a member of the RW Tri or UX UMa subtype of nova-like variables based on these results and because it shows different spectral characteristics at different dates. This spectral behaviour suggests that EC 21178−5417 undergoes distinct variations in mass transfer rate on the observed time-scales of months and years.

Key words: accretion, accretion discs – binaries: close – stars: individual: EC 21178−5417 – novae, cataclysmic variables.

1 INTRODUCTION

Cataclysmic variables (CVs) are interacting binary systems consisting of an electron degenerate star [a white dwarf (WD) primary] and a low-mass secondary star. The secondary star is usually on or near the main sequence, rich in hydrogen, and transfers material on to the WD via a gas stream and accretion disc. In addition, a bright-spot is formed at the intersection of the disc and gas stream. Non-magnetic CVs are classified into two main types, namely dwarf novae (DNe) and nova-like (NL). The former, DNe, show outbursts of 2–8 mag, and are subdivided into U Gem, Z Cam, and SU UMa types (Warner 1995). The latter, NLs, resemble non-eruptive nova remnants and are probably pre-novae, or remnants of pre-historic novae. Thus NLs show no outbursts, but a few of them show DN outbursts and some show low and high states, e.g. DW UMa (Dhillon, Jones & Marsh 1994; Dhillon, Smith & Marsh 2013).

NL variables are disc-dominated CVs characterized by higher mass transfer rates exceeding the expected rates based on standard magnetic braking as angular momentum loss mechanism (Townsley & Gänsicke 2009). NLs show nearly constant accretion luminosity, and are, unlike most other CVs, almost always observed in the outburst state (Noebauer et al. 2010). Thus NLs are like DN in permanent outburst and have orbital periods just above the period gap in the orbital period distribution diagram of non-magnetic CVs (e.g. fig. 18 of Knigge, Baraffe & Patterson 2011), where magnetic braking is thought to reproduce the largest mass transfer rates in the long-term evolution of CVs (Howell, Nelson & Rappaport 2001). NLs show short time-scale spectroscopic and photometric variability that is similar to those of DN between outbursts. Optical spectra of NL show a wide range of distinctive features that depend on a variety of conditions, such as the temperature of the WD,

★ E-mail: khangalezn@saao.ac.za

inclination angle, and mass transfer from the secondary ($\dot{M}_2$). Based on their spectroscopic and photometric behaviour, NLs are classically divided into four distinct subtypes: UX Ursae Majoris (UX UMa), RW Triangulum (RW Tri), SW Sextantis (SW Sex), and VY Sculptoris (VY Scl). Warner (1995) gives a comprehensive review of NLs.

EC 21178−5417 is a 13.7 mag eclipsing NL variable that was discovered in the Edinburgh-Cape Blue Object Survey (Stobie et al. 1997). Its orbital period is ∼3.708 h (Warner, Woudt & Pretorius 2003). This orbital period was confirmed by Zietsman (2008) from high-speed photometric data, where he also analysed spectroscopic data obtained using the Southern African Large Telescope (SALT; Buckley et al. 2006) on 2006 August 17 during the primary eclipse. The average spectrum of EC 21178−5417 was found to reveal strong, broad, and double-peaked emission from He II 4686 Å and Balmer (Hα, Hβ, and Hδ), and other He I lines. Warner et al. (2003) found EC 21178−5417 to be a rich source of dwarf nova oscillations (DNOs) and quasi-periodic oscillations (QPOs). In addition to that, they found EC 21178−5417 to show other types of periodic oscillations called longer period dwarf nova oscillations (lpDNOs). Recent photometry studies of EC 21178−5417 by Bruch (2017) revealed no QPOs or DNOs reported by Warner et al. (2003). However, the observations of Bruch (2017) were taken at lower signal-to-noise ratio. Also, Warner & Nather (1972) and Knigge et al. (1998) noted that for NLs, the DNOs were not always visible in the Fourier transforms (e.g. UX UMa). Warner et al. (2003) estimated the success rate (at least once in a run) for detecting DNOs at 83 per cent for EC 21178−5417.

In this paper, we present an updated ephemeris of EC 21178−5417 based on our full photometric archive of this object, spanning six epochs between 2002 and 2016 (Section 3). We then present in Section 4 a detailed spectroscopic analysis of the original identification spectra (Edinburgh-Cape Blue Object Survey), and follow-up spectra obtained in 2011 and 2013. The latter were obtained during an extended photometric campaign. In Section 5, Doppler tomography of the 2011 and 2013 spectroscopy is presented. This is followed by a brief discussion based on the results in Section 6.

2 OBSERVATIONS

2.1 Photometry

Photometric observations of EC 21178−5417 were obtained by our group from 2002 to 2016 at the South African Astronomical Observatory (SAAO) station in Sutherland using the SAAO 1.9-m Radcliffe Reflector Telescope. The finding chart of EC 21178−5417 is shown in Fig. 1.

2.1.1 UCT CCD photometer

EC 21178−5417 was first observed with the SAAO 1.9-m telescope using the University of Cape Town (UCT) CCD photometer (O'Donoghue 1995) between 2002 September 7 and 2002 November 30. The log of these observations is given in table 1 of Warner et al. (2003). Some of these observations were short runs, not covering the eclipse, so they were not useful in improving the ephemeris. Therefore, they were not used in this paper, only those dates that appears in Table 3 are used. The UCT CCD photometer was operated in its white light (WL) mode in order to capture as many photons as possible. For all these observations, the UCT CCD was used in frame-transfer mode. The integration time of 5, 6, and 10 s were used.

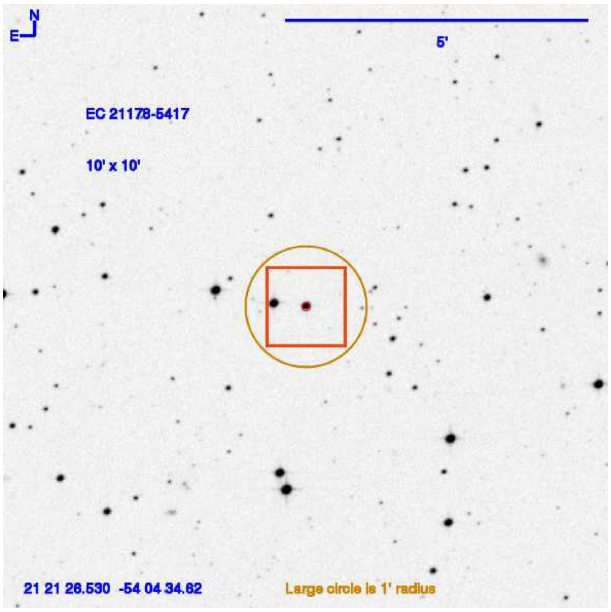

Figure 1. Digital Sky Survey image of the field of view around EC 21178−5417. The field of view of the Sutherland High-speed Optical Camera (SHOC) camera [1.29 × 1.29 arcmin^2 for the South African Astronomical Observatory (SAAO) 1.9-m] is indicated with the red square and our target centre of the square and the comparison star is on the left. The orange circle marks 1 arcmin radius circle around the target star.

The data were reduced following the recipes of O'Donoghue (1995) and the resulting magnitudes calibrations and extinctions corrections are only approximations. The magnitudes derived in this case are approximate scale and were derived with the use of hot WDs standards (Landolt 1992). Therefore, our magnitudes approximate to a V scale to ∼0.1 mag. It is worth noting that the average mean out of eclipse magnitude (V) of this target ranged between 13.6 and 13.8. A total of nine eclipses resulted from these observations.

EC 21178−5417 was observed again with the SAAO 1.9-m telescope using the UCT CCD photometer (O'Donoghue 1995) over four consecutive nights in 2006 August 16–19. Full description of these observations is given in Zietsman (2008).[1] We have reproduced the log of observations from Zietsman (2008) and is given in Table 1. The UCT CCD photometer was equipped with a Johnson V filter and the detectors were used in frame-transfer mode. An integration time of 6 s was selected. These observations included at least one complete eclipse per run. We have rereduced the 2006 data following the procedures described in O'Donoghue (1995). Since these observations were filtered, we calibrated our observations to the Sloan r photometric system (see Coppejans et al. 2014 for more details). We compared the calibration offset using hot WDs with those obtained using Sloan Digital Sky Survey (SDSS) photometry of the comparison star. It was found that there was a stable zero-point offset of 0.12 ± 0.05 mag between V and SDSS r. A total of seven eclipses were obtained from the 2006 data.

[1]For more details see https://open.uct.ac.za/handle/11427/4412

Table 1. Photometric observations log.

Run no.	Date (start of night)	HJD of first obs (+245 0000.0)	Length (h)	t_{in} (s)	Filter used	Telescope used	Instrument used
S7651	2006 Aug 16	3964.28141	5.35	6	*V*	SAAO 1.9-m	UCT CCD
S7655	2006 Aug 17	3965.32565	6.26	6	*V*	SAAO 1.9-m	UCT CCD
S7659	2006 Aug 18	3966.31921	4.36	6	*V*	SAAO 1.9-m	UCT CCD
S7661	2006 Aug 19	3967.40985	0.74	6	*V*	SAAO 1.9-m	UCT CCD
S8097	2011 Oct 5	5840.27376	4.12	0.5	WL	SAAO 1.9-m	SHOC

Note. HJD is the Heliocentric Julian Date, t_{in} is the integration time, *V* is the Johnson *V* filter, and WL is white light or unfiltered mode.

2.1.2 *SHOC observations*

Follow-up photometric observations of EC 21178−5417 were made with the SAAO 1.9-m telescope on the night of 2011 October 5 using the Sutherland High-speed Optical Camera (SHOC; Coppejans et al. 2013) for the purpose of refining the ephemeris. A record of observation is given in Table 1. EC 21178−5417 was observed for a duration of 4.12 h, and a total of two eclipses, one complete and the other a partial eclipse, were covered by the observations. The observations were made in WL (unfiltered) mode. The SHOC camera was mounted below the filter wheel of the 1.9-m reflector telescope. The field of view is 1.29 × 1.29 arcmin^2 (see Fig. 1), and the data were binned 8 × 8 for a plate scale of 0.61 arcsec pixel^{-1}. Sky flat-fields were obtained at the beginning of the night with the same binning of the CCD. The exposure time was selected to be 0.5 s and the detector was used in frame transfer mode. The 1 MHz electron-multiplying (EM) mode was used with an EM gain of 20 and a pre-amplifier gain of 7.5 e$^-$ pixel^{-1}. An effective read noise ∼1 e$^-$ pixel^{-1} is achieved by using these settings. The camera was thermoelectrically cooled at −70°C, resulting in a dark current of <0.001 e$^-$ pixel^{-1}.

The photometric data of EC 21178−5417 were reduced using the IRAF[2] data reduction package. EC 21178−5417 and a comparison star were identified on each image with the IRAF task DAOFIND, and aperture photometry was obtained for both stars, using PHOT in the DAOPHOT package. Multiple apertures were used and an aperture correction was applied using MKAPFILE in IRAF (Stetson 1990). We determined the brightness of the comparison star as $r' = 13.07$ mag from simultaneous g', r', and i' photometry using the three-colour imaging camera (TRIPOL) on the SAAO 0.75-m telescope.

For the final light curve (Fig. 2), a differential correction was applied to the photometry of EC 21178−5417 by assuming that the comparison star in the field is constant and has a brightness of $r' = 13.07$ mag. Even though our observations are taken in WL mode, the details of variability and eclipse depth of EC 21178−5417 match that of the light curve in r' band obtained by Dr Nagayama with TRIPOL at the same time. Note that these observations were taken for the purpose of determining the precise time of mid-eclipse so precise photometry calibration was not essential. A total of two eclipses were obtained from the 2011 observations.

At the end of the observation campaign, a total of 18 eclipses were obtained from these observations and we measured their mid-eclipse times and the results are listed in Table 3. All the mid-eclipse times were corrected for the light-travel-time effect to the barycentre of the Solar system [i.e. converted to the Barycentric Dynamical Times (TDB) as Barycentric Julian Date (BJD; Eastman, Siverd & Gaudi 2010)].

[2]IRAF is distributed by the National Optical Astronomy Observatories, which are operated by the Association of Universities for Research in Astronomy, Inc., under cooperative agreement with the National Science Foundation (NSF).

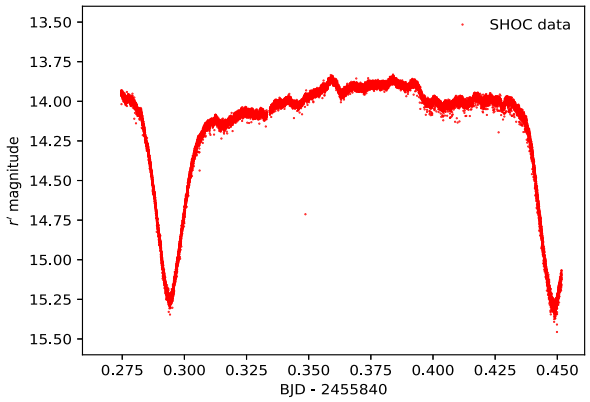

Figure 2. Photometric light curve of EC 21178−5417 obtained from our 2011 October 5 observations, showing the deep eclipse.

2.1.3 *Other observations*

EC 21178−5417 was observed on eight separate nights between 2015 July 14 and 2016 May 12 (see Bruch 2017 for details of these observations). A total of 10 eclipses were observed (see Table 3), they measured 10 mid-eclipse times. A further eclipse of EC 21178−5417 was observed on 2016 July 19 with the SHOC instrument on the SAAO 1.9-m telescope (see Ruiz-Carmona et al. 2020 for more details on this observations). Their mid-eclipse time is given in Heliocentric Julian Date (HJD) and we converted this to BJD. We combined all the mid-eclipse times from the literature (e.g. Bruch 2017; Ruiz-Carmona et al. 2020) with our 18 mid-eclipse times as to bring the final total to 29 mid-eclipse times and they are shown in Table 3.

2.2 Spectroscopy

Observations of EC 21178−5417 were made with the SAAO 1.9-m telescope using the grating spectrograph over nine nights stretching from 2002 September 7 until 2013 October 22. Table 2 provides our spectroscopic observing log. Our spectroscopic observations were made during good sky conditions, i.e. good seeing and low humidity. The Scientific Imaging Technologies, Inc. (SITe) CCD was used and the spectra were pre-binned 1 × 2. A slit width of 1.5 arcsec was used. Grating 6 was used for most of the observations (2002, 2011 October, and 2013) with a central wavelength of ∼4400 Å, and a wavelength range of 3500–5400 Å. The grating angle was set to ∼14°.1, giving a reciprocal dispersion of 1.11 Å pixel^{-1}. For the spectra obtained on 2011 September 5, a lower resolution grating

Table 2. Spectroscopic observation log of EC 21178−5417.

Date of observation	Number of spectra	Exposure time (s)	Grating angle (°)	Central wavelength (Å)	Wavelength range (Å)	Orbital phase coverage
2002 Sept 7*	7	600	14.1	4400	3500–5400	0.76–1.25
2011 Sept 5	24	600	17.2	5700	3550–7500	0.41–1.61
2011 Oct 22	12	900	14.1	4400	3500–5400	0.85–1.72
2011 Oct 23	12	900	14.1	4400	3500–5400	0.30–1.15
2013 Oct 16	20	900	14.1	4400	3500–5400	0.58–1.97
2013 Oct 17	14	900	14.1	4400	3500–5400	0.94–1.87
2013 Oct 18	20	900	14.1	4400	3500–5400	0.41–1.79
2013 Oct 19	22	900	14.1	4400	3500–5400	0.85–2.35
2013 Oct 22	18	900	14.1	4400	3500–5400	0.34–1.56

Note. The asterisk '∗' sign marks the observations retrieved from the archive.

(Grating 7) was used so that the central wavelength was ∼5700 Å, with a wavelength range of 3600–7600 Å. The grating angle was set to ∼17.°2, giving a reciprocal dispersion of 2.29 Å pixel^{-1}. This includes the Hα line, telluric lines towards the red, and the spectral range previously covered. The exposure time for each spectrum was selected to be 600 s, or 900 s, for the various observing runs (see Table 2). These exposure times allow a sufficient phase resolution and coverage of the orbital cycle. For the purposes of flux calibration, the following standard stars were observed: EG 21, LTT 7987 and 7379, and HR 1544. Several spectra were taken in such a way that they cover one orbital cycle of the binary on each night, each separated by one or two Cu–Ar arc spectra with the exposure time of ∼30 s.

The spectroscopic data of EC 21178−5417 were reduced following standard procedures using IRAF data reduction package. The frames were first overscanned, trimmed, and then flat-fielded with a master flat-field. The spectra were extracted using IRAF's implementation of optimal extraction using APALL task. The arc spectra were extracted at the position of the corresponding object spectrum and were then used to wavelength calibrate the target spectra by interpolation between neighbouring arcs. The spectra were corrected for instrumental response using the flux standard stars mentioned above. All the spectra were transformed to heliocentric rest frame and corrected for local atmospheric extinction. The final average one-dimensional spectrum for each date is presented in Fig. 4.

3 PHOTOMETRY

3.1 Photometric ephemeris

The light curve of EC 21178−5417 (Fig. 2) obtained on 2011 October 5 shows deep symmetrical V-shaped primary eclipse minima, with out-of-eclipse magnitudes of ∼13.8 mag and a depth of the primary eclipse of about 1.3 mag. The average magnitude out of eclipse of EC 21178−5417 is consistent with previous observations made for this system in 2002 and 2006 (Warner et al. 2003; Zietsman 2008). The total width of the eclipse is ∼0.1 in orbital phase. There is some short time-scale variability present in the light curve, but this appears to be mere flickering. No DNOs or QPOs (reported by Warner et al. 2003) were detected in the 2011 October observations.

We used the mid-eclipse time from 2006 October 16 as the starting point, T_0, and used the orbital period from Zietsman (2008) to calculate the cycle numbers. Table 3 gives all the 29 mid-eclipse times of EC 21178−5417. After using a linear least-squares fit to the above-mentioned timings, we determined the following orbital ephemeris:

$$\mathrm{BJD_{min}} = 245\,3964.3323\ (\pm 1 \times 10^{-4}) + 0.15452724\ (\pm 1 \times 10^{-8})\mathrm{E}. \quad (1)$$

Fig. 3 shows the observed minus calculated (O − C) diagram after subtraction of the best-fitting (straight line) ephemeris based on the data outlined in Table 3. The best-fitting results to the residuals can be obtained by using a quadratic or cubic ephemeris to the mid-eclipse times. This will significantly reduce the residuals seen in Fig. 3. We note that the scatter of eclipse times within each epoch and

Table 3. Eclipse timings of EC 21178−5417 (given in BJD-TDB-245 0000) and cycle numbers.

Date of start of night	Time of mid-eclipse (240 0000+)	Error in time of eclipse	Cycle number	Reference
2002 Sept 7	52525.375126	0.0001	−9312	[a]
2002 Sept 7	52525.529546	0.0001	−9311	[a]
2002 Oct 1	52549.480922	0.0001	−9156	[a]
2002 Oct 3	52551.335181	0.0001	−9144	[a]
2002 Oct 4	52552.416912	0.0001	−9137	[a]
2002 Oct 6	52554.271978	0.0001	−9125	[a]
2002 Oct 8	52556.280912	0.0001	−9112	[a]
2002 Oct 9	52557.361865	0.0001	−9105	[a]
2002 Nov 30	52609.283881	0.0001	−8769	[a]
2006 Aug 16	53964.33115	0.000047	0	This work
2006 Aug 16	53964.48625	0.000067	1	This work
2006 Aug 17	53965.41375	0.000055	7	This work
2006 Aug 17	53965.56825	0.000058	8	This work
2006 Aug 18	53966.34075	0.000066	13	This work
2006 Aug 18	53966.49495	0.000087	14	This work
2006 Aug 19	53967.422849	0.000049	20	This work
2011 Oct 5	55840.294147	0.000054	12 140	This work
2011 Oct 5	55840.448878	0.000062	12141	This work
2015 July 14	57217.74883	0.0001	21 054	[b]
2015 Aug 11	57245.562940	0.0001	21 234	[b]
2015 Aug 11	57245.717880	0.0001	21 235	[b]
2015 Aug 12	57246.64511	0.0001	21 241	[b]
2015 Aug 12	57246.79950	0.0001	21 242	[b]
2015 Aug 13	57247.72708	0.0001	21 248	[b]
2015 Aug 14	57248.65353	0.0001	21 254	[b]
2015 Aug 15	57249.73531	0.0001	21 261	[b]
2016 May 10	57518.76817	0.0001	23 002	[b]
2016 May 12	57520.77724	0.0001	23 015	[b]
2016 July 19	57589.541596	0.00002	23 460	[c]

[a]Warner et al. (2003); [b]Bruch (2017); [c]Ruiz-Carmona et al. (2020).

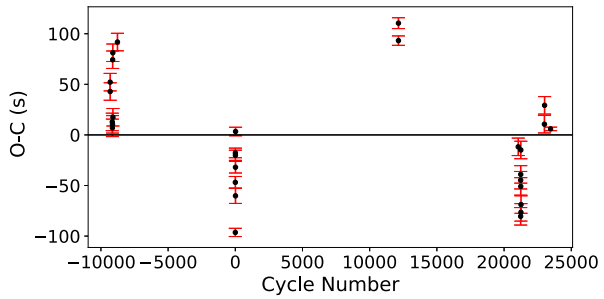

Figure 3. Observed minus calculated eclipse time residuals after subtraction of the eclipse ephemeris (equation 1).

the total time span of our data set do not warrant additional terms. The individual error bars in Fig. 3 are formal errors from fitting a Gaussian to the eclipse profile. The scatter within each epoch suggests that variability (e.g. flickering) is adding an additional random contaminant to measuring the true centre of the eclipse. This ephemeris (equation 1) was used to phase all of our spectroscopic data.

3.2 System's inclination and dimensions

We now use the eclipse length and the orbital period of the system in order to estimate the mass ratio, inclination, and the masses of the stellar components. In order to estimate the orbital inclination, we consider the geometry of a point eclipsed by a spherical body. It is possible to determine the inclination, i, of a binary system through the relation

$$\left(\frac{R_2}{a}\right)^2 = \sin^2(\pi\Delta\varphi_{1/2}) + \cos^2(\pi\Delta\varphi_{1/2})\cos^2 i, \quad (2)$$

where R/a is the volume radius of the secondary star and $\Delta\varphi_{1/2}$ is the mean phase full width of the eclipse at half the out-of-eclipse intensity. According to equation (2) of Eggleton (1983), the volume radius of the secondary star depends only on the mass ratio, $q = M_2/M_1$, as shown below:

$$\frac{R_2}{a} = \frac{0.49\,q^{2/3}}{0.6\,q^{2/3} + \ln(1+q^{1/3})}. \quad (3)$$

We calculated $\Delta\varphi_{1/2}$ from the individual light curves covering complete eclipse. We took the average of the eclipse widths and the derived value is $\Delta\varphi_{1/2} = 0.092 \pm 0.003$.

The mass of the secondary star can be estimated using the mean empirical mass–period relationship, i.e. equation (9) from Smith & Dhillon (1998), as follows:

$$M_2(\mathrm{M}_\odot) = (0.126 \pm 0.011)P - (0.11 \pm 0.04) = 0.36(\pm 0.08),$$

where P is the orbital period expressed in hours. For stable mass transfer we require that $M_2/M_1 < 1$ and, therefore, using the above estimate of M_2 (=0.36 $\mathrm{M}_\odot$), the mass of the primary must be within the range $0.36 < M_1 < 1.44$ $\mathrm{M}_\odot$. This as an equivalent of $0.25 < q = M_2/M_1 < 1$. However, according to Gänsicke (1997) and Smith & Dhillon (1998), the average mass of the WD in CVs above the period gap is ∼0.8 $\mathrm{M}_\odot$ (e.g. HS 0728+6738; Rodríguez-Gil et al. 2004). In order for us to provide an estimate of the uncertainty for the orbital inclination, we will assume that the true mass of the primary lies in the range 0.6-1.0 $\mathrm{M}_\odot$ (i.e. $0.36 < q < 1.0$). Taking this into account we obtain an orbital inclination of $83^\circ \pm 7^\circ$. The uncertainty in i include systematic ones from the use of mass–period relation and from the assumption of an axially symmetric accretion disc. The statistical uncertainties in the measurement of $\Delta\varphi_{1/2}$ is then negligible.

4 SPECTRAL ANALYSIS

4.1 Averaged spectra of EC 21178−5417

The averaged continuum-normalized spectrum of EC 21178−5417 obtained over four different epochs is shown in Fig. 4 (top and bottom panels), and is quite remarkable in its detail and wealth of features. The blue spectrum (Fig. 4, top panel) is dominated by the emission line from He II 4686 Å (strongest feature). The strength of the He II 4686 Å emission line is typical of a NL system with a high rate of mass transfer (Szkody et al. 2004). The Balmer lines (Hβ, Hγ, Hδ down to H10) are clearly present with an increasing absorption component towards the blue end of the spectrum. Balmer emission was more pronounced in 2011 October in Hβ, Hγ, Hδ, and Hϵ. The He I lines (at 4026, 4471, 4921, and 5015 Å) all have a strong absorption component. The Bowen (C III/N III) blend at 4640–4650 Å and C II at 4267 Å are clearly seen in emission. In addition, the blue spectrum shows absorption and emission of He II (at 4200 and 4542 Å, part of the He II Pickering series) and absorption from Mg I at 5175 Å. Also visible are the Ca II lines (at 3933 and 3969 Å) towards the blue part of the spectrum in absorption.

The red spectrum (Fig. 4, bottom panel) is dominated by double-peaked Hα emission: a typical signature of disc emission due to the Doppler shifting of orbiting disc material; He II 5411 Å and He I at 5875 and 6678 Å are seen in emission with an absorption core. There is a clear evidence for an asymmetry in the line profile (more specifically in Hα line), suggesting that emission from another location within the system contributes. This has been seen in other CVs (e.g. detached WD/M-dwarf binaries) in low states, where they originate either on or close to the WD (e.g. Tappert et al. 2007, 2011; Parsons et al. 2012, 2013) or from material located between the two stars (e.g. Gänsicke et al. 1998; O'Donoghue et al. 2003; Parsons et al. 2011).

In the top panel of Fig. 4, we show and compare the average continuum-normalized blue spectra of EC 21178−5417 obtained from the four different dates: 2002 September (red), 2011 September (black), 2011 October (blue), and 2013 October (magenta). The average spectrum of EC 21178−5417 from 2002 September (Fig. 4) is dominated by emission from He II 4686 Å and the Balmer lines with very little absorption from He I lines. This is similar to the average spectrum obtained from the 2013 October observations (Fig. 4). This suggests that EC 21178−5417 was in a similar state during the 2002 September and 2013 October observations. On the other hand, the average spectrum obtained in 2011 September (Fig. 4) show strong absorption from the Balmer (from Hγ down to H10) and He I lines (e.g. He I 4471 Å). Even the Hβ itself has a strong absorption component. This suggest that EC 21178−5417 was caught in a distinct state in 2011 September compared to that of 2002 September and 2013 October. The average spectrum obtained in 2011 October (Fig. 4) exhibits both absorption and emission features. Noticeable are broad and double-peaked emission features from Hβ and Hγ, which suggest that these lines originate in an accretion disc. The blueshifted peaks of Hβ and Hγ are stronger than the redshifted peaks. This effect has been observed in other CVs such as the DN V2051 Oph (Steeghs et al. 2001) but they did not attempt an interpretation other than that the blue side of the accretion disc could be making a larger contribution to the emission. The Hδ and Hϵ lines show similar behaviour to that of Hβ and Hγ, but for the former, the redshifted peak appears in absorption.

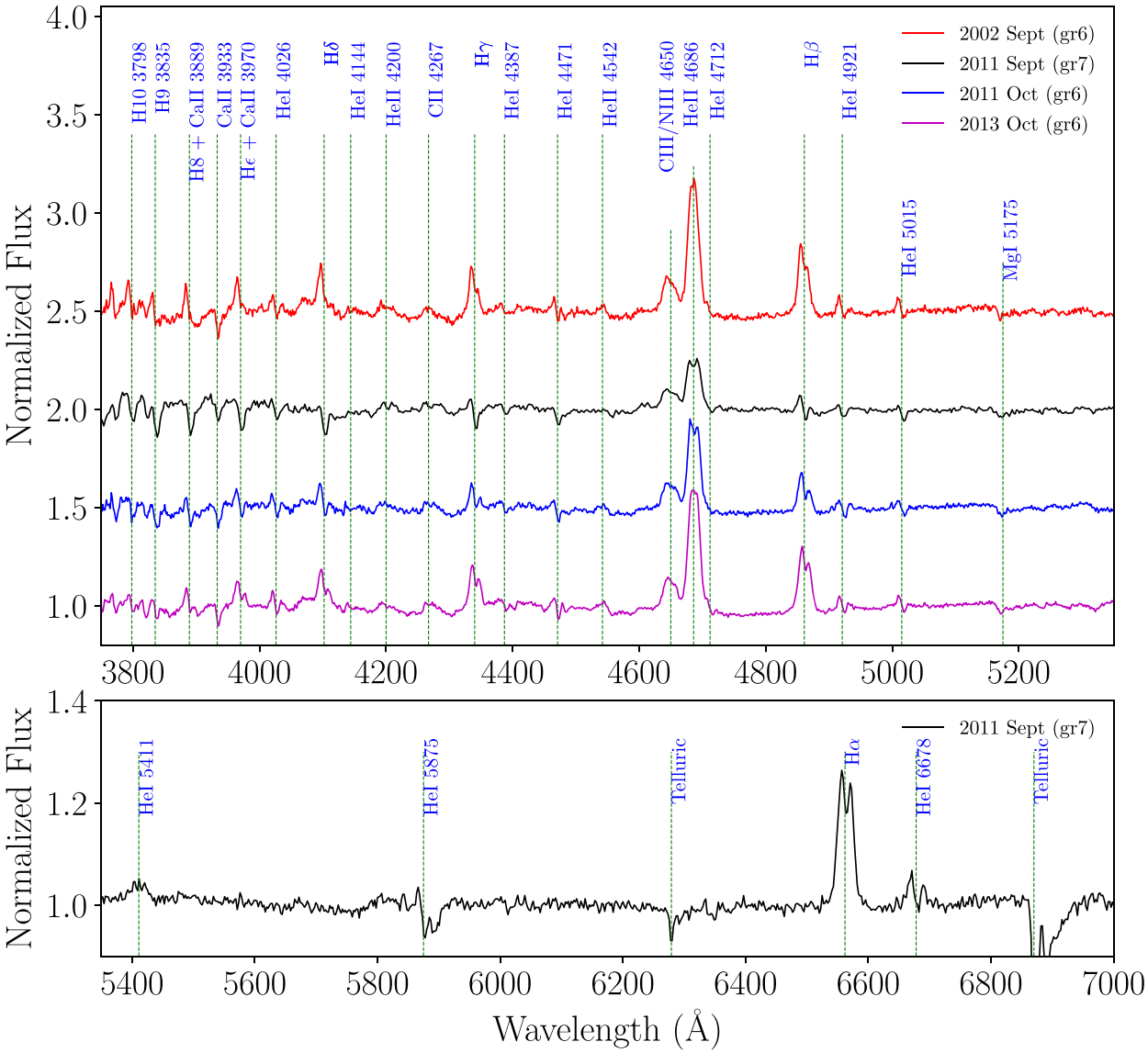

Figure 4. Averaged continuum-normalized spectra of EC 21178−5417, in which each individual spectrum is given equal weighting, obtained from four different dates. Top panel (from top to bottom): spectrum from 2002 September (red), 2011 September (black), 2011 October (blue), and 2013 October (magenta). Each spectrum in the top panel is shifted up by increment of 0.5 from the bottom to top. The bottom panel shows the red averaged spectrum from 2011 September. The prominent lines have been identified and labelled in each panel.

The averaged spectra of EC 21178−5417 show distinct spectral features depending on various factors such as the state of the accretion disc, mass transfer rate, etc., which seem to vary on time-scales of months and years (see Fig. 4). For example, the 2011 October spectra (Fig. 4) show the intermediate state, where both emission and absorption are present. Thus this system changes from mostly emission (2002 September) to absorption (2011 September), and then to intermediate state a month later in 2011 October. But 2 yr later, 2013 October, the average spectrum is again dominated by emission. This is somewhat unexpected given that the out-of-eclipse brightness of EC 21178−5417 is similar throughout the individual observation runs. This could be attributed to a change in mass transfer rate between the individual observations but could also be due to the varying strength of the absorption component. The other spectral features that are present also vary from one observation to the other.

4.2 The bright-spot spectrum

Fig. 5 shows the average flux-calibrated spectrum of EC 21178−5417 at three different phase bins: before the eclipse ($0.75 \leq \phi < 0.95$), during the eclipse ($0.95 \leq \phi < 0.05$), and out-of-eclipse ($0.05 \leq \phi < 0.75$). It is clear from the figure that the spectrum changes substantially with orbital phase. The continuum shape of the spectrum obtained during mid-eclipse (bottom of Fig. 5) is slightly flatter than the other two; this was also noted by Zietsman (2008). The Balmer series, He II 4686 Å, He I lines, and C III/N III blend are present and double-peaked in emission. The strength of the He II 4686 line and the C III/N III blend at 4650 Å are reduced during eclipse, whereas that of the Balmer lines are enhanced. This indicates that the former lines originate close to the WD and the inner accretion disc, and they are more affected by the eclipse.

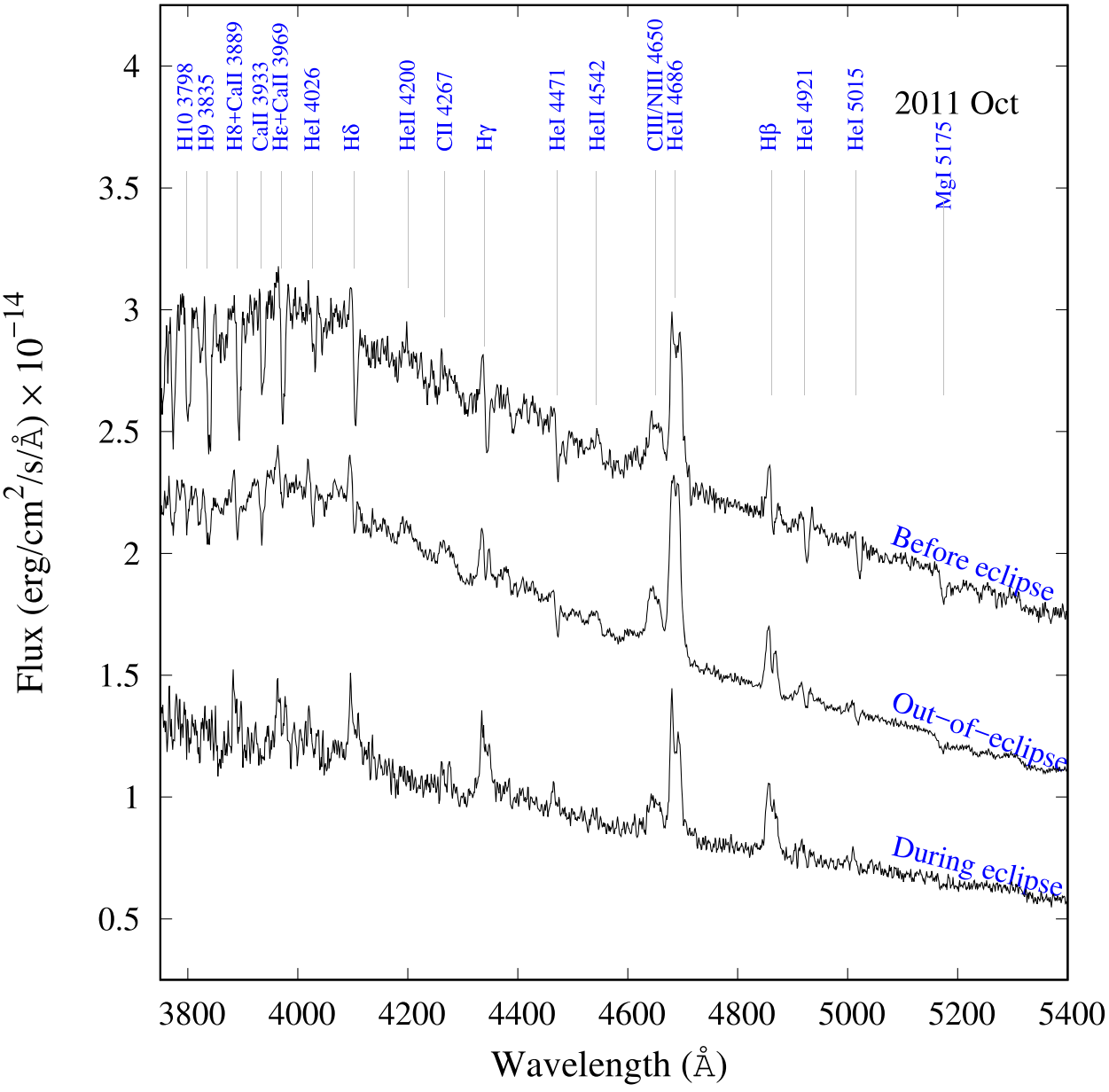

Figure 5. Averaged spectra of EC 21178−5417 at phase intervals $0.75 \leq \phi < 0.95$ (top, offset by $+7.0 \times 10^{-15}$), $0.05 \leq \phi < 0.75$ (middle), and $0.95 \leq \phi < 1.05$ (bottom). The prominent lines have been marked and labelled.

The out-of-eclipse spectrum of EC 21178−5417 (Fig. 5, middle) is similar to the average spectrum shown in Fig. 4 (top panel, blue line) with strong and broad double-peaked emission lines from He II 4686 Å and the Balmer lines. He I lines and C III/N III blend are also present in broad emission and/or absorption on a steep continuum. The ratio of He II 4686 Å to Hβ is larger than unity, and the presence of He II 5411 Å suggests that these emission lines are formed in a region with a higher than usual level of ionization (Groot, Rutten & van Paradijs 2001).

The spectrum of EC 21178−5417 obtained before the eclipse (Fig. 5, top) revealed that the higher Balmer lines (Hϵ to H10) change from general emission at phases $0.05 \leq \phi < 0.75$ to absorption at phases $0.75 \leq \phi < 0.95$. This has been observed during the low states of SW Sex (Groot et al. 2001) and UX UMa (Neustroev et al. 2011), and is attributed to contribution from the bright-spot. Thus the higher Balmer lines likely originate from the vicinity of the bright-spot that is clearly visible at phases $0.75 \leq \phi < 0.95$ (see fig. 15 of Groot et al. 2001). The high excitation features, He II 4686 Å, C III/N III blend at 4650 Å, and C II 4267 Å, do not change in strength compared to the continuum and each other. However, Hβ, Hγ, and Hδ, each have two components: the redshifted absorption peak and the blueshifted emission peak. But the absorption is stronger than the emission, which is the opposite of what was seen for Hδ and Hϵ at earlier phases. Furthermore, the He I lines also change from emission and broad absorption to strong absorption.

5 DOPPLER TOMOGRAPHY

5.1 Trailed spectra of the line profiles

The middle and right-hand panels of Figs 6–9 show continuum-normalized and phase-binned trailed spectra (observed and recon-

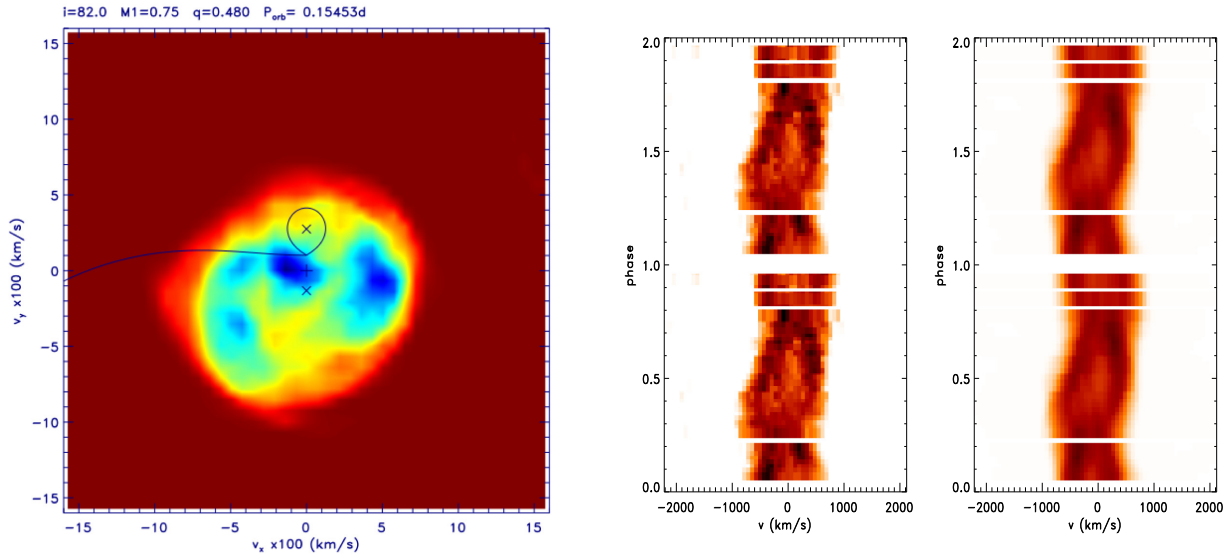

(a) HeII 4686 Å line (2011 October 22-23)

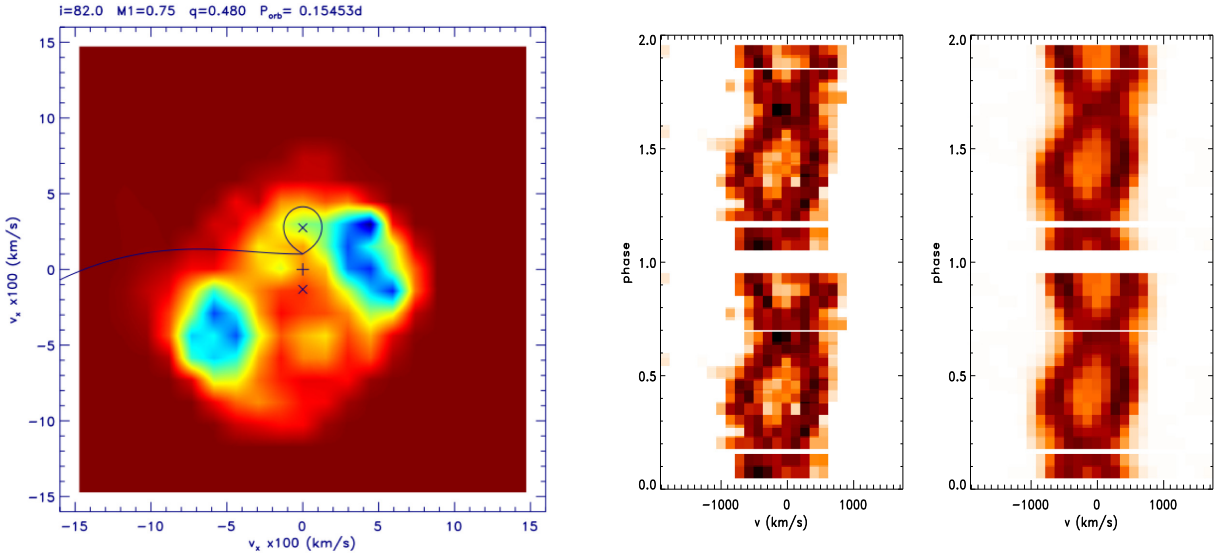

(b) HeII 4686 Å line (2011 September 5)

Figure 6. Doppler maps (left-hand panels), trailed observed (centre panels), and reconstructed (right-hand panels) spectra of He II 4686 Å emission lines.

structed) of He II 4686 Å, the Balmer lines, and He I 4471 Å, respectively. The reconstructed spectra are constructed based on features shown in the Doppler maps. The agreement between the observed and reconstructed trailed spectra serves as a measure of the reliability of the Doppler maps. The trailed spectra of He II 4686 Å show two peaks moving in antiphase with respect to each other, whereas that of the Balmer lines (and He I) show two peaks moving in-phase with each other.

The observed trailed spectra of He II 4686 Å lines from the 2011 observations (Figs 6a and b, middle panels) show two peaks in emission separated by ∼1000 km s^{-1} at phase 0.0 with the semi-amplitude of ∼600 km s^{-1}. The two peaks move in antiphase direction with respect to each other. At phase ∼0.2, the two peaks come to within 200 km s^{-1} of each other; it is not clear if these two peaks swap side. But at about phase ∼0.7, the redshifted peak crosses the zero velocity from red to blue, whereas the blueshifted peak crosses the zero velocity from blue to red (see Figs 6a and b, middle panels). Similarly, the middle panel of Fig. 8(a) shows the trailed spectra of He II 4686 Å obtained after subtracting the average spectrum from the individual spectra taken in 2013 October. This is the main reason why the trailed spectra of He II 4686 Å in Figs 6 and 8 appear different. The reconstructed trailed spectra for He II 4686 Å lines (right-hand panels of Figs 6a and b) show consistent results with the observed trailed spectra and are similar to those of IP Peg for the same line (Harlaftis et al. 1999). The only difference is the absence of the third central peak in emission (associated with the secondary star)[3] in the trailed spectra of He II 4686 Å of EC 21178−5417, which is present for IP Peg. The reconstructed trailed spectra in the right-hand

[3]This central feature is associated with the secondary star and is seen as an S-wave in the trailed spectra. It is most common in DNe during outbursts and is thought to be due to the irradiation of the secondary star, e.g. IP Peg (Harlaftis et al. 1999).

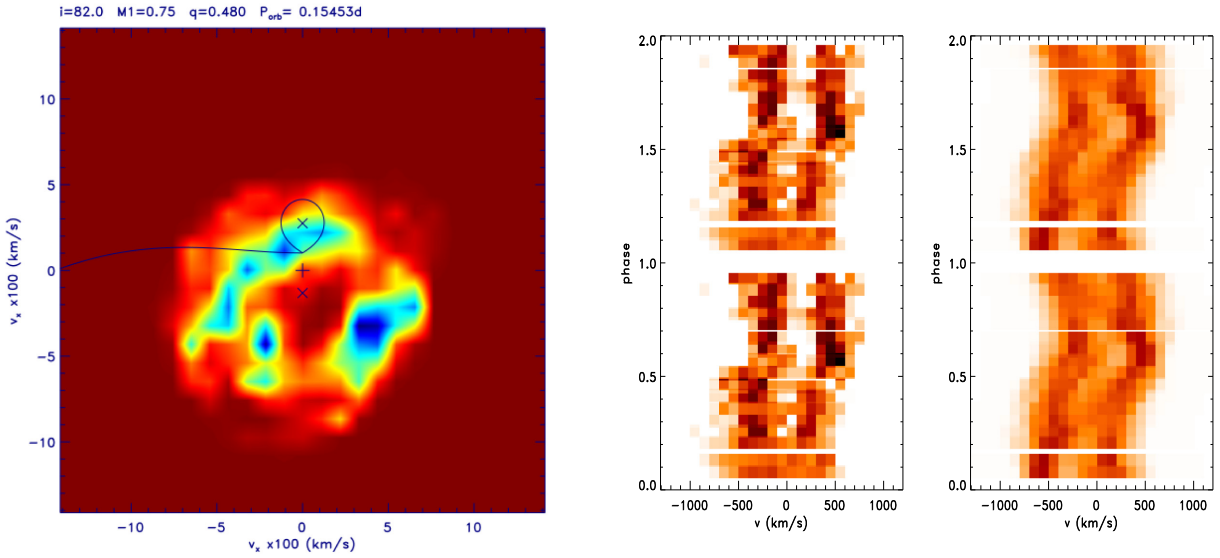

(a) Hα line (2011 September 5)

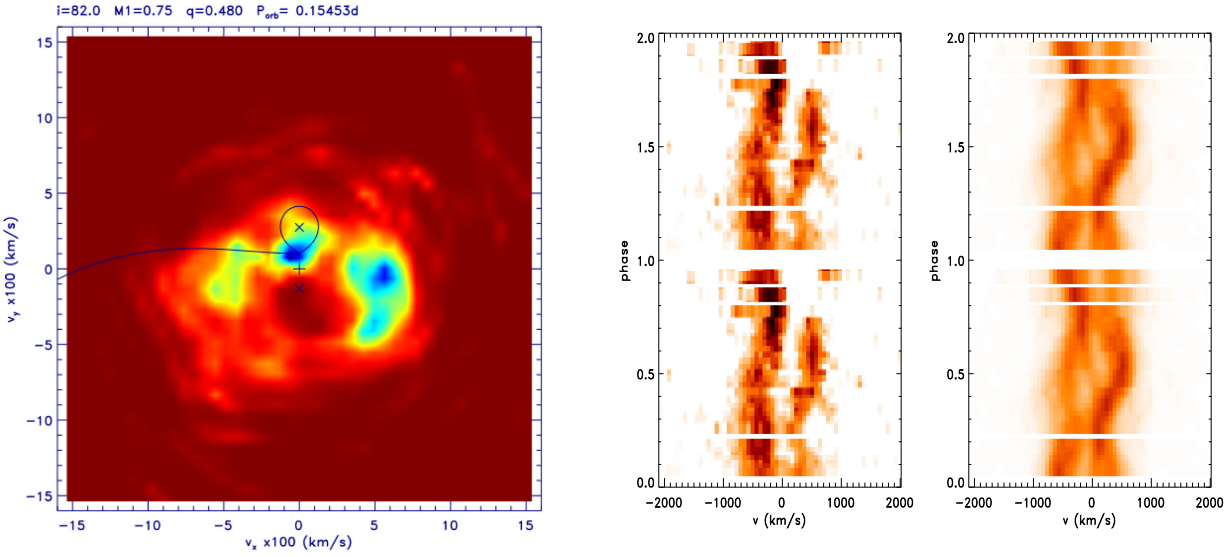

(b) Hβ line (2011 October 22-23)

Figure 7. Doppler maps (left-hand panels), trailed observed (centre panels), and reconstructed (right-hand panels) spectra of the Hα and Hβ emission lines.

panel of Fig. 8(a) are also consistent with the observed trailed spectra.

Fig. 7(a) (middle panel) shows the observed trailed spectra of the Hα line from 2011 September 5 data. There are two emission peaks that are clearly visible throughout the orbital cycle. For this line, the two emission peaks are moving in-phase with respect to each other. As with the He II 4686 lines, the observed trailed spectra of the Hα line do not show any emission that is attributed to the secondary star. This is evident by the absence of the central emission feature seen in the trailed spectra of IP Peg during outbursts (Steeghs, Harlaftis & Horne 1997). The reconstructed trailed spectra of this line are also consistent with the observed trailed spectra.

The observed trailed spectra of the Hβ line from 2011 October (Fig. 7b, middle panel) and 2013 October (Fig. 8b, middle panel) resemble that of the Hα line. There are two emission peaks that are clearly visible and moving in-phase with each other. The central absorption dip is present in Hβ. However, at $\phi \sim 0.7$, the second peak disappear or switches to absorption and reappears at $\phi \sim 0.9$. The reconstructed spectra of the Hβ line (Figs 7b and 8b) show two peaks moving in antiphase with respect to each other. It is not clear if the two peaks cross the zero velocity.

Lastly, the observed and reconstructed trailed spectra of Hγ are presented in Fig. 9(a) (middle and right-hand panels) and show similar results with those of the Hβ line. The observed trailed spectra of He I 4471 Å are also shown in Fig. 9(b). It shows a mixture of absorption and emission and is difficult to interpret. The reconstructed spectra of He I 4471 Å do not reproduce the input spectra.

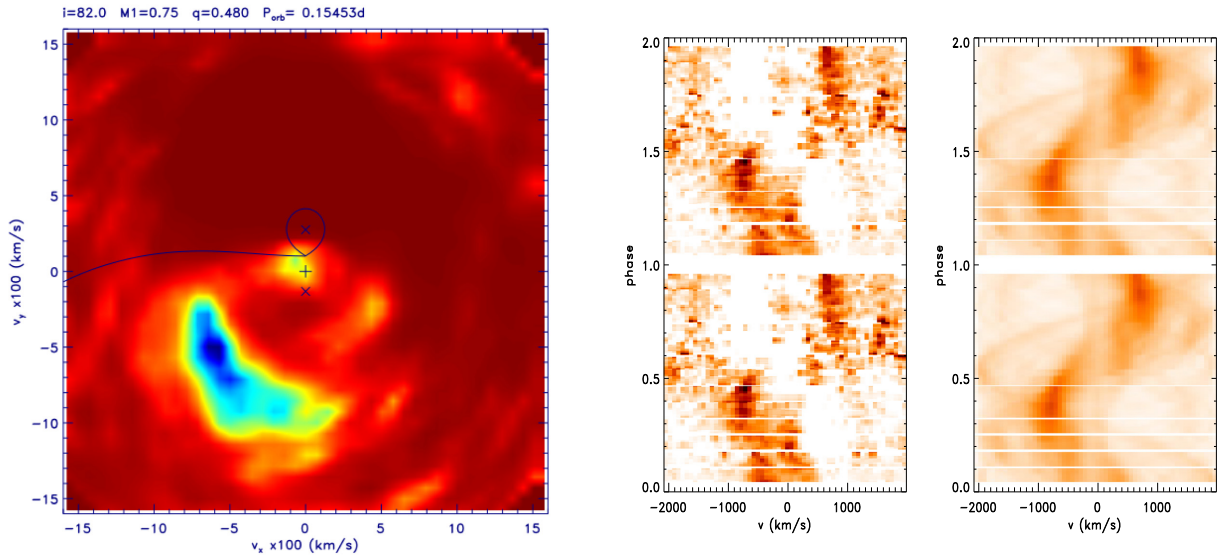

(a) HeII 4686 Å line (2013 October 16-22)

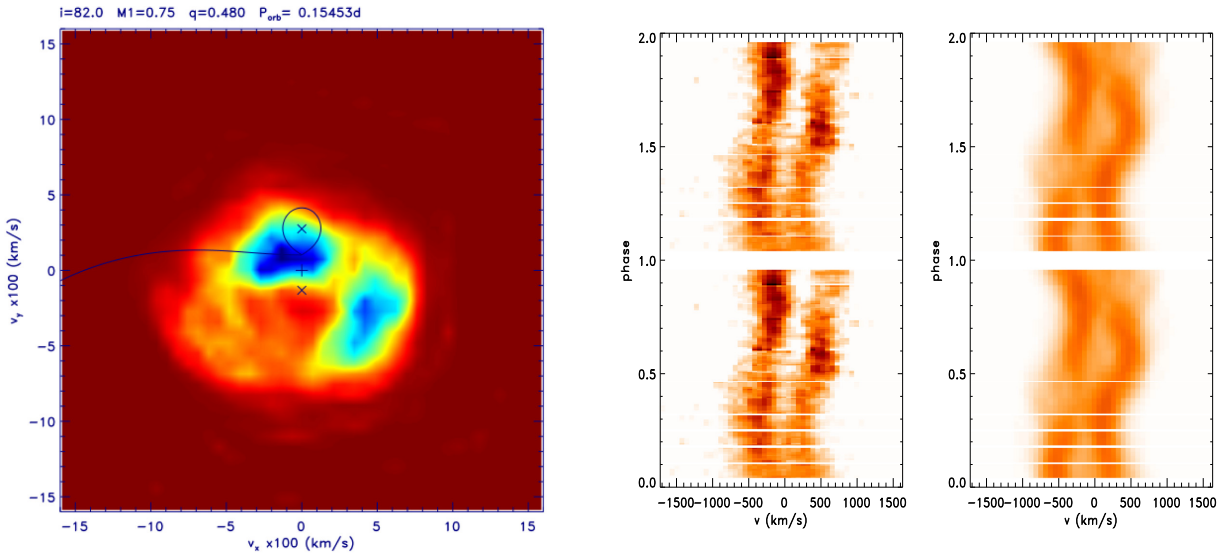

(b) Hβ line (2013 October 16-22)

Figure 8. Doppler maps (left-hand panels), trailed observed (centre panels), and reconstructed (right-hand panels) spectra of He II 4686 Å and Hβ emission lines.

5.2 Doppler maps

We constructed Doppler maps of EC 21178−5417 using the fast maximum entropy method (FMEM)[4] code developed by Spruit (1998) that uses IDL[5] for plotting. We used the mass of the secondary star ($M_2 = 0.36$ M$_\odot$) and the inclination (i) of 82° and assumed that the mass of the WD primary (M_1) to be ∼0.75 M$_\odot$ (e.g. Gänsicke 1997; Smith & Dhillon 1998). These gives the mass ratio, $q = M_2/M_1 = 0.48$ and the orbital period ($P_{\rm orb} = 0.154527$ d) given in equation (1). These parameters were used to compute the Roche lobe and the stream overlaid on the Doppler maps. The location of the primary and secondary is indicated with a '×', whereas that of the centre of mass of the binary is marked with a '+'. Similarly, the location of the accretion stream trajectory is indicated by a solid blue line and marks the trajectory followed by the materials moving at stream velocity. The Roche lobe of the secondary star is also indicated. The Doppler maps of EC 21178−5417 are shown in Figs 6–9 for the 2011 and 2013 observations. For the 2011 observations, the trailed spectra used for the Doppler maps were rebinned into 20 phase bins of 0.05 each. The 2013 observations were rebinned into 40 bins of 0.025 each. The velocity resolution was approximately the same for each observations and was around 70 km s^{-1} pixel^{-1}.

The left-hand panel of Figs 6(a) and (b) show the Doppler maps obtained from the He II 4686 Å lines. The two panels reveal an asymmetric accretion disc. Also, there is evidence of a spiral

[4]See http://www.mpa-garching.mpg.de/~henk/pub/dopmap/ for more details.

[5]The acronym IDL stands for Interactive Data Language and is a trademark of ITT and/or Exelis Visual Information Solutions. For further details see http://www.exelisvis.com/ProductsServices/IDL.aspx

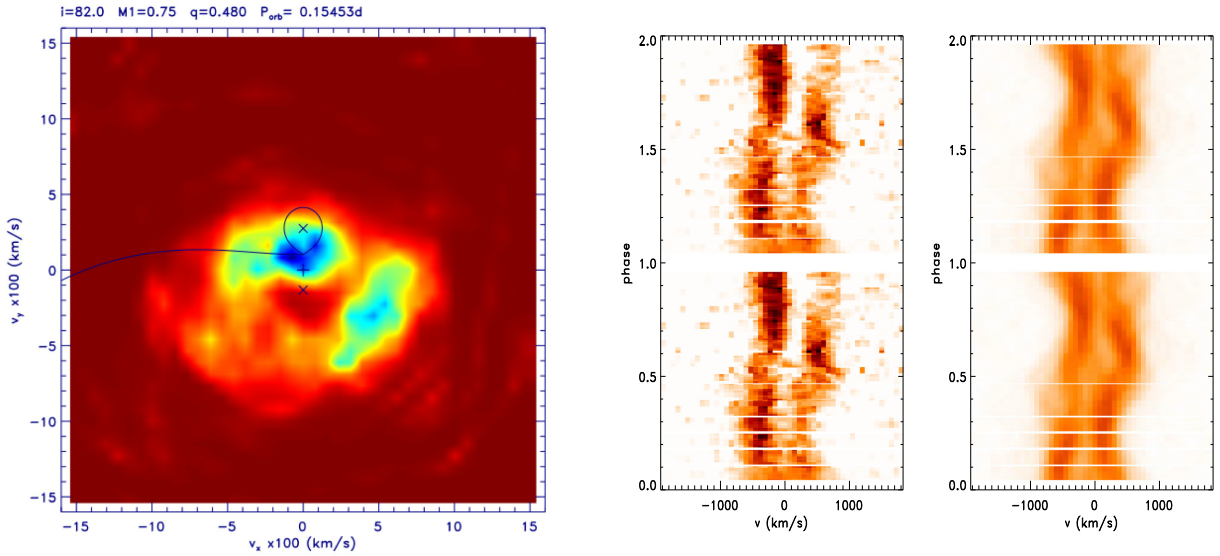

(a) Hγ line (2013 October 16-22)

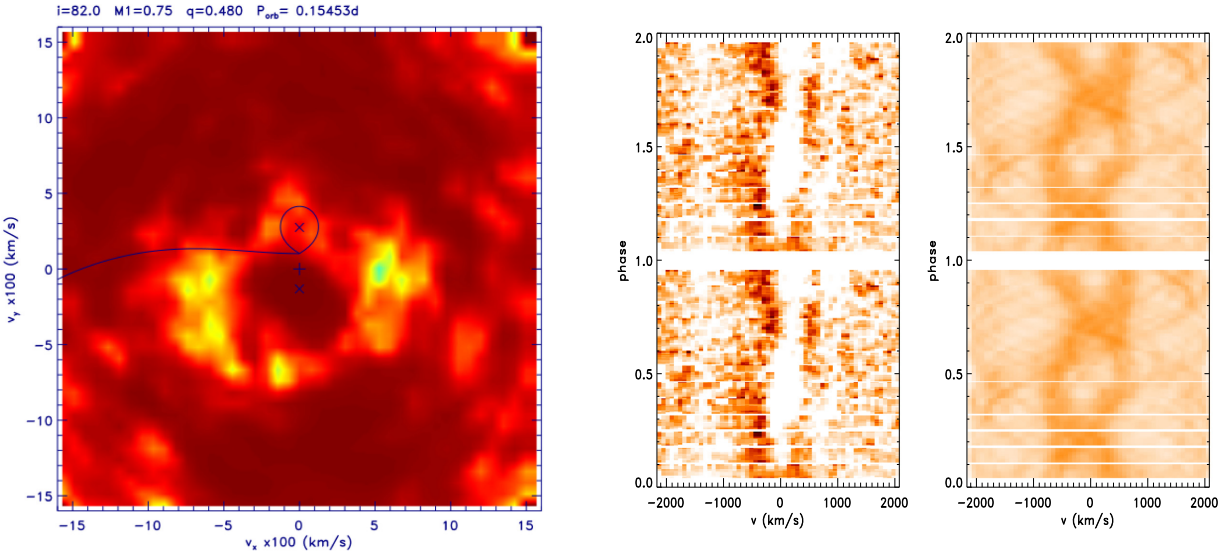

(b) HeI 4471 Å line (2013 October 16-22)

Figure 9. Doppler maps (left-hand panels), trailed observed (centre panels), and reconstructed (right-hand panels) spectra of the Hγ and He I 4471 Å emission lines.

structure that is interpreted as the indication of the presence of the tidally induced shock waves in the accretion disc such as that observed during outbursts in the DN IP Peg (Steeghs et al. 1997; Harlaftis et al. 1999; Steeghs & Stehle 1999; Morales-Rueda, Marsh & Billington 2000). There is a strong two-armed disc asymmetry visible, especially in Fig. 6(a), which is reminiscent of the two-armed spiral structure in the accretion disc. The emission in Fig. 6(b) is concentrated in the first and third quadrant, and result from the effect of spiral density waves in the accretion disc. The non-equal emission of the two sides of the asymmetry lends some support to the models of Smak (2001). But there is emission from the region between the WD and the secondary in Fig. 6(a) that makes the Doppler map difficult to interpret. This feature is seen in the Doppler map from the 2011 October observations. We noted that the He II 4686 Å phase binned spectra from this date (fig. 4.9 of Khangale 2013) showed multiple components and we therefore associate the emission between the WD and the secondary star to one of the components.

Similarly, Fig. 8(a) shows the Doppler map obtained after subtracting the average spectrum from the individual spectra obtained on 2013 October 16–22. The main reason for doing this was to recover the spiral structure like those shown in Fig. 6 for the same line. The original Doppler map of He II 4686 Å from 2013 October observations showed a blob centred on the WD and it was difficult to interpret. It is clear from Fig. 8(a) that the Doppler map is elongated and contains a spiral structure in the third quadrant. The second arm of the spiral structure is weak, i.e. at a noise level.

Doppler maps of the Balmer lines, left-hand panel of Figs 7(a) and (b) and left-hand panel of Figs 8(b) and 9(a), also suggest an asymmetric accretion disc similar to that of He II 4686 Å line but with less defined spiral structure. In general, the Doppler maps of the Balmer lines reveal a more circular accretion disc. The Doppler

map of the Hα line (Fig. 7a) shows no evidence of the emission associated with irradiated secondary, whereas that of Hβ (Figs 7b and 8b) and Hγ (Fig. 9a) lines suggests that there could be emission from the secondary star. But, the reality of this feature in the Doppler map of Hβ and Hγ is questionable (see Section 5.1). A possible reason for the absence of the distinct spiral structure in the Doppler map of the Balmer lines is that these lines are more strongly affected by the additional absorption component in the lines, making the Doppler maps difficult to interpret. Further, no bright-spot emission is seen in the Doppler maps of the Balmer lines. Fig. 9(b) shows the Doppler map of He I 4471 Å that is consistent with that of He II 4686 Å and the Balmer lines. However, most of the features are not clearly visible. As expected, no emission from either the hotspot or the secondary star is present on the Doppler map of He I 4471 Å.

6 DISCUSSION AND CONCLUSION

The spectroscopic results presented in Sections 4 and 5 followed from nine nights worth of observations of EC 21178−5417 covering at least one orbital cycle of the binary system per night. Analysis of the spectroscopic results of EC 21178−5417 reveals that it is dominated by double-peaked emission lines from a highly inclined accretion disc. The strength of the He II 4686 Å for EC 21178−5417 is similar and/or comparable to that seen during the outbursts of IP Peg (Marsh & Horne 1990). The ratio of He II 4686 Å to Hβ is greater than unity and the presence of He II 5411 Å suggests that these two lines originate from the region that has higher than normal level of ionization, e.g. SW Sex (Groot et al. 2001). Further, the presence of He II at 4200 Å and C II at 4267 Å that are seen during DNe outbursts suggest that EC 21178−5417 is characterized by high mass transfer rate.

In the last paragraphs of Section 4.1 we compared the average spectrum of EC 21178−5417 taken at different observational dates. It shows different spectral characteristics at different dates: from pure absorption in the Balmer lines (2011 September) through mixed absorption and emission in the Balmer and He I lines (2011 October) to pure line emission (2002 September and 2013 October). This change in spectral features from emission to absorption is attributed to variability of the mass transfer rate from the secondary star to the WD, or, at times EC 21178−5417 is dominated by an additional absorption component associated with the bright-spot. Recently, UX UMa was reported to show similar variations on a yet undetermined time scale (Neustroev et al. 2011). We have seen that the bright-spot appears strong at $0.75 \leq \phi \leq 0.95$ (Section 4.2), and the higher Balmer lines change to absorption when the bright-spot is visible. This short-lived absorption comes from a vertically extended region above the bright-spot (Groot et al. 2001). Based on these characteristics alone we may conclude that EC 21178−5417 is a member of either the RW Tri or UX UMa class of NLs since the double-peaked emission lines rule out the SW Sex membership.

The trailed spectra of He II 4686 Å lines show two peaks moving in antiphase, whereas that of the Balmer lines show two peaks moving in-phase with each other (see Section 5.1). The antiphase direction between the two peaks results from a spiral structure or wave in the accretion disc. The observed and reconstructed trailed spectra of EC 21178−5417 were consistent between the three observations, except for the Hβ and Hγ line that suggested a third component with low velocity amplitude – that is associated with emission from the secondary star. This is attributed to one of the Doppler tomography axioms that state that the intensity of the line emission remains constant throughout the orbital phase. The Doppler tomography code has added a third component to compensate for this varying line emission.

Doppler maps of He II 4686 Å for EC 21178−5417 (Section 5.2) reveal the presence of an asymmetric and highly inclined accretion disc with spiral structures. The asymmetry and non-equal intensity of the two regions of emissions are similar to that observed in some DN during outbursts, e.g. IP Peg (eg. Steeghs & Stehle 1999; Morales-Rueda et al. 2000), SS Cyg (Steeghs et al. 1996; Kononov et al. 2012), EX Dra (Joergens et al. 2000a; Joergens, Spruit & Rutten 2000b), U Gem (e.g. Groot 2001), and WZ Sge (Baba et al. 2002; Steeghs 2004). In NLs, spiral structure has been seen in the Doppler maps of three other systems, e.g. V347 Pup (Still, Buckley & Garlick 1998; Thoroughgood et al. 2005), V3885 Sgr (Hartley et al. 2005), and UX UMa (Neustroev et al. 2011). This makes EC 21178−5417 the fourth NL to show spiral structure in its Doppler map. But in previous three systems, spiral structures were seen in the Balmer and He I lines. The spiral structures found in EC 21178−5417 are similar to those found in the Doppler maps of IP Peg (e.g. Steeghs et al. 1997; Harlaftis et al. 1999) and EX Dra (Joergens et al. 2000b) during outbursts. More specifically, the spiral arms in the He II 4686 Å line of EX Dra do not follow a circle centred on the WD but are rather elongated along the (V_x, V_y) axis, the same hold for EC 21178−5417 (see Figs 6 and 8). The Doppler maps of the Balmer lines reveal a more circular accretion disc, and are harder to interpret due to the time variable absorption component. There is no emission from the secondary star in the Doppler maps of the Balmer lines and the blob/spot in the vicinity of the secondary is either an extension of the disc or the spiral structure. Also, there is no evidence of emission from near the WD in the Doppler maps of EC 21178−5417.

In summary, we presented spectroscopic analysis and Doppler tomography of the eclipsing NL EC 21178−5417. It has shown persistent spiral structure in its Doppler maps on three occasions and is now one of the four NLs binary systems after V347 Pup, V3885 Sgr, and UX UMa to show spiral density waves in its tomograms. A follow-up study on the night-to-night behaviour of the spiral structures in EC 21178−5417 has been conducted by Ruiz-Carmona et al. (2020).

ACKNOWLEDGEMENTS

We would like to thank the anonymous referee whose comments were helpful and improved our paper. ZNK acknowledges the postgraduate bursary from the National Research Foundation (NRF) of South Africa through National Astrophysics and Space Science Programme (NASSP) and the internship from the Department of Science and Innovation of South Africa (Ref. No.: S703-8000-887) leading to these results. PAW and BW acknowledge financial support from the NRF and the University of Cape Town (UCT). DK acknowledges the University of the Western Cape (UWC) and the NRF for financial support.

REFERENCES

Baba H. et al., 2002, PASJ, 54, L7
Bruch A., 2017, New Astron., 56, 60
Buckley D. A. H., Burgh E. B., Cottrell P. L., Nordsieck K. H., O'Donoghue D., Williams T. B., 2006, in Ian S. M., Masanori I., eds, Proc. SPIE 6269, Ground-based and Airborne Instrumentation for Astronomy. p. 62690A
Coppejans R. et al., 2013, PASP, 125, 976
Coppejans D. L. et al., 2014, MNRAS, 437, 510
Dhillon V. S., Jones D. H. P., Marsh T. R., 1994, MNRAS, 266, 859

Dhillon V. S., Smith D. A., Marsh T. R., 2013, MNRAS, 428, 3559
Eastman J., Siverd R., Gaudi B. S., 2010, PASP, 122, 935
Eggleton P. P., 1983, ApJ, 268, 368
Gänsicke B. T., 1997, PhD thesis, Universität Göttingen
Gänsicke B. T., Hoard D. W., Beuermann K., Sion E. M., Szkody P., 1998, A&A, 338, 933
Groot P. J., 2001, ApJ, 551, L89
Groot P. J., Rutten R. G. M., van Paradijs J., 2001, A&A, 368, 183
Harlaftis E. T., Steeghs D., Horne K., Martín E., Magazzú A., 1999, MNRAS, 306, 348
Hartley L. E., Murray J. R., Drew J. E., Long K. S., 2005, MNRAS, 363, 285
Howell S. B., Nelson L. A., Rappaport S., 2001, ApJ, 550, 897
Joergens V., Mantel K.-H., Barwig H., Bärnbantner O., Fiedler H., 2000a, A&A, 354, 579
Joergens V., Spruit H. C., Rutten R. G. M., 2000b, A&A, 356, L33
Khangale Z. N., 2013, Master's thesis, Univ. Cape Town
Knigge C., Long K. S., Wade R. A., Baptista R., Horne K., Hubeny I., Rutten R. G. M., 1998, ApJ, 499, 414
Knigge C., Baraffe I., Patterson J., 2011, ApJS, 194, 28
Kononov D. A., Giovannelli F., Bruni I., Bisikalo D. V., 2012, A&A, 538, A94
Landolt A. U., 1992, AJ, 104, 340
Marsh T. R., Horne K., 1990, ApJ, 349, 593
Morales-Rueda L., Marsh T. R., Billington I., 2000, MNRAS, 313, 454
Neustroev V. V., Suleimanov V. F., Borisov N. V., Belyakov K. V., Shearer A., 2011, MNRAS, 410, 963
Noebauer U. M., Long K. S., Sim S. A., Knigge C., 2010, ApJ, 719, 1932
O'Donoghue D., 1995, Balt. Astron., 4, 519
O'Donoghue D., Koen C., Kilkenny D., Stobie R. S., Koester D., Bessell M. S., Hambly N., MacGillivray H., 2003, MNRAS, 345, 506
Parsons S. G., Marsh T. R., Gänsicke B. T., Tappert C., 2011, MNRAS, 412, 2563
Parsons S. G. et al., 2012, MNRAS, 419, 304
Parsons S. G., Marsh T. R., Gänsicke B. T., Schreiber M. R., Bours M. C. P., Dhillon V. S., Littlefair S. P., 2013, MNRAS, 436, 241
Rodríguez-Gil P., Gänsicke B. T., Barwig H., Hagen H. J., Engels D., 2004, A&A, 424, 647
Ruiz-Carmona R., Khangale Z. N., Woudt P. A., Groot P. J., 2020, MNRAS, 491, 344
Smak J. I., 2001, Acta Astron., 51, 295
Smith D. A., Dhillon V. S., 1998, MNRAS, 301, 767
Spruit H. C., 1998, preprint (arXiv:astro-ph/9806141)
Steeghs D., 2004, Astron. Nachr., 325, 185
Steeghs D., Stehle R., 1999, MNRAS, 307, 99
Steeghs D., Horne K., Marsh T. R., Donati J. F., 1996, MNRAS, 281, 626
Steeghs D., Harlaftis E. T., Horne K., 1997, MNRAS, 290, L28
Steeghs D., O'Brien K., Horne K., Gomer R., Oke J. B., 2001, MNRAS, 323, 484
Stetson P. B., 1990, PASP, 102, 932
Still M. D., Buckley D. A. H., Garlick M. A., 1998, MNRAS, 299, 545
Stobie R. S. et al., 1997, MNRAS, 287, 848
Szkody P. et al., 2004, AJ, 128, 1882
Tappert C., Gänsicke B. T., Schmidtobreick L., Aungwerojwit A., Mennickent R. E., Koester D., 2007, A&A, 474, 205
Tappert C., Gänsicke B. T., Schmidtobreick L., Ribeiro T., 2011, A&A, 532, A129
Thoroughgood T. D. et al., 2005, MNRAS, 357, 881
Townsley D. M., Gänsicke B. T., 2009, ApJ, 693, 1007
Warner B., 1995, Cataclysmic Variable Stars. Cambridge Univ. Press, Cambridge
Warner B., Nather R. E., 1972, MNRAS, 159, 429
Warner B., Woudt P. A., Pretorius M. L., 2003, MNRAS, 344, 1193
Zietsman E., 2008, Master's thesis, Univ. Cape Town

This paper has been typeset from a TEX/LATEX file prepared by the author.